$\alpha + {}^{15}$O cluster structure in ^{19}Ne and resonant α scattering

R. Otani,[1] R. Kageyama,[1] M. Iwasaki,[1] M. Kudo,[1] M. Tomita,[1] and M. Ito[1,2]
[1]*Department of Pure and Applied Physics, Kansai University, Yamatecho, 3-3-35, Suita, Japan*
[2]*Research Center for Nuclear Physics (RCNP), Osaka University, Mihogaoka 10-1, Suita 567-0047, Japan*
(Received 16 January 2014; revised manuscript received 1 September 2014; published 23 September 2014)

The rotational bands of $\alpha + {}^{15}\mathrm{O}(1/2^-)$ in ^{19}Ne are calculated by employing a simple potential model. The $\alpha - {}^{15}$O interaction potential is constructed from the calculation of the $^{20}\mathrm{Ne} = \alpha + {}^{16}$O structure and the $\alpha + {}^{15}$N elastic scattering. The resonant levels and their decay width are identified by imposing the absorbing boundary condition. The present calculations predict the sequence of the discrete and overlapping resonances in the negative- and positive-parity states of ^{19}Ne, respectively. The excitation function of the $\alpha + {}^{15}$O elastic scattering is also calculated, and the appropriate condition to observe the resonances is discussed.

DOI: 10.1103/PhysRevC.90.034316 PACS number(s): 21.60.Gx, 24.10.Eq, 25.60.Je, 27.20.+n

I. INTRODUCTION

The α cluster structures have been extensively studied for the so-called $4N$ nuclei with $N = Z$, such as $^8\mathrm{Be} = 2\alpha$, $^{12}\mathrm{C} = 3\alpha$, $^{16}\mathrm{O} = \alpha + {}^{12}$C, and $^{20}\mathrm{Ne} = \alpha + {}^{16}$O [1–3]. In current studies, the importance of the cluster degrees of freedom has been extended to the neutron-rich ($N > Z$) systems, which are obtained by adding extra neutrons to the $4N$ cluster systems. In the neutron-rich systems, such as $^{12}\mathrm{Be} = 2\alpha + 4N$ [4], $^{16}\mathrm{C} = 3\alpha + 4N$ [5], and $^{22}\mathrm{Ne} = \alpha + {}^{16}\mathrm{O} + 2N$ [6], various chemical-bonding-like structures are generated by the coupling of the cluster relative motion and the single-particle motion of extra neutrons. In particular, the drastic structure changes among the chemical-bonding-like states are pointed out in the continuum energy region of ^{12}Be [4].

In contrast, cluster structures in the $4N$ systems with a hole in a cluster core are also interesting research subjects [7–10]. For example, there is a recent study of $^{11}\mathrm{B} = \alpha + \alpha + t$, corresponding to a proton hole system of $^{12}\mathrm{C} = 3\alpha$ [7]. Pioneering work of the cluster plus nucleon-hole system is the study of the ^{19}F nucleus [8–10]. The ^{19}F nucleus is the one-proton-deficient system of ^{20}Ne, and the rotational bands of $\alpha + {}^{15}$N and $t + {}^{16}$O, which are calculated from the folding-type potentials, were clearly assigned to the energy levels observed in the α and t transfer reactions [8]. The excited levels in ^{19}F have also been analyzed in the more sophisticated models, such as the full microscopic alpha-hole cluster model [9] and the coupled channel of $(\alpha + {}^{15}\mathrm{N}) + (t + {}^{16}\mathrm{O})$ [10]. In the analysis of Ref. [10], t and α cluster bands are clearly identified, although a considerable mixture of these two configurations occurs.

In the $\alpha + {}^{15}$N system, a proton hole inside of the ^{16}O cores weakly couples to the relative motion of the binary cluster cores. In a naive consideration, the weak coupling scheme of the hole in ^{16}O and the α particle is also expected in the neutron-deficient system, $\alpha + {}^{15}$O in ^{19}Ne. In fact, a formation of $\alpha + {}^{15}$O in ^{19}Ne was discussed from the perspective of ^{19}F-^{19}Ne Coulomb displacement energy [8,10]. However, detailed analysis of the energy levels over a wide energy region, which contain the analysis of the resonance width above the α threshold and the excitation function of the resonant scattering, have not been undertaken yet because available experimental data are still limited. Therefore, a study of the $\alpha + {}^{15}$O cluster structure in ^{19}Ne, corresponding to the $N < Z$ system, is very interesting from the viewpoint of the systematics of the clustering phenomena in the $N \neq Z$ systems.

There is another reason why we focus on the $\alpha + {}^{15}$O structure in the ^{19}Ne nucleus. The $^{15}\mathrm{O}(\alpha,\gamma)^{19}\mathrm{Ne}$ reaction is known to play a crucial role in the advanced stages of astrophysical hydrogen burning [11]. At characteristic nova temperatures ($0.2\ \mathrm{GK} \leqslant \mathrm{T} \leqslant 0.5\ \mathrm{GK}$), it is currently expected that the $^{15}\mathrm{O}(\alpha,\gamma)^{19}\mathrm{Ne}(p,\gamma)^{20}\mathrm{Na}(\beta^+,\nu)^{20}\mathrm{Ne}$ reaction sequence is the predominant breakout channel from the hot carbon-nitrogen-oxygen (CNO) cycle to the rapid proton capture (rp) process, where the energy generation rate can increase by two orders of magnitude [12]. In the $^{15}\mathrm{O}(\alpha,\gamma)^{19}\mathrm{Ne}$ reaction, the most crucial resonance is known to arise through the $3/2^+$ resonance level at 504 keV with respect to the $\alpha + {}^{15}$O threshold ($E_x = 4.03$ MeV). Unfortunately, direct measurement of the resonance at 504 keV is still difficult because of the small strength of the resonance and its energy position extremely close to the α decay threshold.

The level assignments and the evaluation of the α decay width (Γ_α) in ^{19}Ne, which are essential quantities in astrophysical calculations, have been extensively done by the transfer reactions [13–17]. For example, the spectroscopic factor of an α particle (S_α) is derived from the experiments on ^{19}F, such as $^{15}\mathrm{N}(^6\mathrm{Li},d)^{19}\mathrm{F}$ [15,16] and $^{15}\mathrm{N}(^7\mathrm{Li},t)^{19}\mathrm{F}$ [17], and the Γ_α in ^{19}Ne is speculated by assuming the mirror symmetry of ^{19}Ne and ^{19}F [18]. The results of Γ_α and S_α are updated in Ref. [19]. The analyses in Refs. [14,15] have pointed out that the intrinsic structure of the resonance at 504 keV in ^{19}Ne is not the $\alpha + {}^{15}$O cluster structure, but the five-particle–two-hole ($5p$-$2h$) configuration with the $^{14}\mathrm{O}_{g.s.}$ core. This result is very interesting because the $\alpha + {}^{15}$O structure is expected to emerge for the excitation energy near the corresponding threshold for decay, $E_x = 4.03$ MeV, according to the threshold rule of Ikeda [20]. Since the $^5\mathrm{He} + {}^{14}$O cluster state largely overlaps with the $5p$-$2h$ configuration in the shell model limit, the coupling of this cluster configuration is important in handling the resonance formation at $E_x = 4.03$ MeV in the $\alpha + {}^{15}$O radiative capture.

In view of this information, we believe that the study of the $\alpha + {}^{15}$O cluster structures is important for understanding the systematics of the α cluster structures as well as for its

 ©2014 American Physical Society

strong impact on astrophysical phenomena. In this article, we investigate the rotational band structures in $\alpha + {}^{15}\mathrm{O}$, based on the potential model similar to the approach by Buck *et al.* [8]. The interaction potential of $\alpha + {}^{15}\mathrm{O}$ is constructed from the structure calculation of ${}^{20}\mathrm{Ne} = \alpha + {}^{16}\mathrm{O}$ [21], and it is tuned so as to reproduce the angular distribution of the $\alpha + {}^{15}\mathrm{N}$ elastic scattering. In particular, we focus on the resonant levels, generated from the high spin states in ${}^{20}\mathrm{Ne}$, by imposing the absorbing boundary condition (ABC) [22–24]. Furthermore, we also calculate the excitation function of the $\alpha + {}^{15}\mathrm{O}$ resonant scattering. The resonant scattering of the radioactive ion (RI) beam has been developed in recent experiments [25] and hence the scattering experiment using the RI beam of ${}^{15}\mathrm{O}$ will be an important tool in future studies. In fact, a resonance identification in the ${}^{15}\mathrm{O}$ scattering by an α target has been done [26]. We predict the excitation function of the $\alpha + {}^{15}\mathrm{O}$ scattering under the same condition of recent experiments [25]. Theoretical analysis on the decay width and the excitation function has not been done in the previous works [8–10].

Of course, in a precise treatment of ${}^{19}\mathrm{Ne}$, the microscopic cluster model [1,2,4], in which the $\alpha + {}^{15}\mathrm{O}$, ${}^{3}\mathrm{He} + {}^{16}\mathrm{O}$, and ${}^{5}\mathrm{He} + {}^{14}\mathrm{O}$ configurations are explicitly coupled, should be performed. However, a simple potential model is still useful to obtain the qualitative feature of the $\alpha + {}^{15}\mathrm{O}$ structure before applying the full microscopic cluster model.

The organization of this article is as follows: In Sec. II, the construction of the interaction potentials for the $\alpha + {}^{15}\mathrm{O}$ system and the method of ABC are briefly explained. In Sec. III, the energy spectra and the rotational band structure in $\alpha + {}^{15}\mathrm{O}$ is shown. In the final part of Sec. III, the excitation function of the $\alpha + {}^{15}\mathrm{O}$ elastic scattering is also calculated under a condition similar to the recent experiment [25]. The final section is devoted to a summary and discussion.

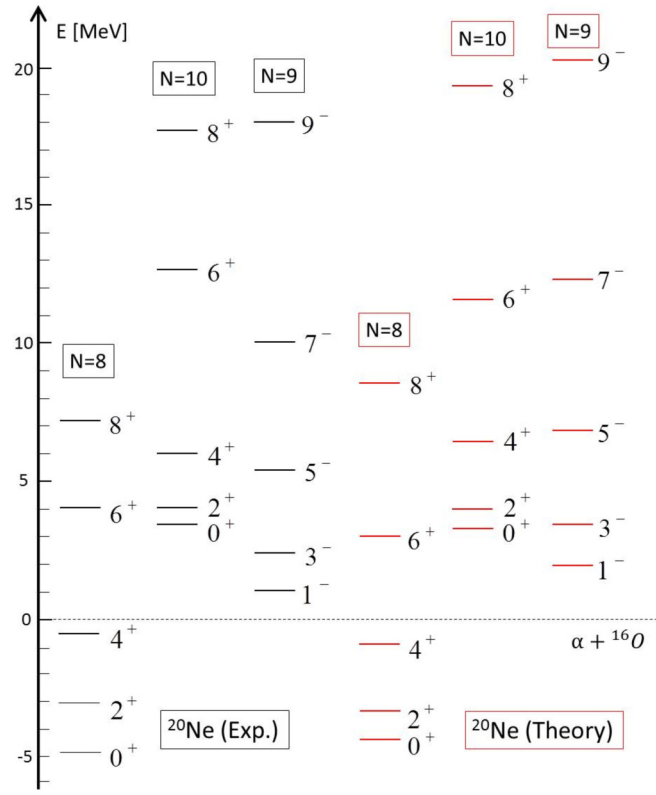

FIG. 1. (Color online) Energy spectra of ${}^{20}\mathrm{Ne}$. The left three groups of the levels represent the experimental spectra, while the right levels show the theoretical calculation obtained by the $\alpha + {}^{16}\mathrm{O}$ cluster model. In individual groups, the left, middle, and right levels have the $N = 8$, 10, and 9, respectively, where N denotes the total oscillator quanta of the harmonic oscillator potential.

II. FRAMEWORK

A. Construction of the α-^{15}O interaction potential

First, we calculate the energy spectra of ${}^{20}\mathrm{Ne} = \alpha + {}^{16}\mathrm{O}$. The $\alpha + {}^{16}\mathrm{O}$ cluster model with a simple potential is known to describe both the ground and excited bands with a natural parity [1,2,8,21]. The Woods-Saxon (WS) potential is assumed for the $\alpha - {}^{16}\mathrm{O}$ nuclear interaction, and its parameters, such as strength V, radius R, and the diffuseness a, are optimized so as to reproduce the observed spectra of the ground band and the excited band with the negative parity. The obtained parameters are $V = -169.21$ MeV, $R = 2.52$ fm, and $a = 0.796$ fm. The radial form of the potential calculated with this parameter set is similar to the folding type interaction used in the $\alpha + {}^{16}\mathrm{O}$ OCM calculation [21]. The Coulomb potential is calculated by assuming the uniform charge distribution with the same radius R as the nuclear potential.

The comparison of the experimental spectra of ${}^{20}\mathrm{Ne}$ with the theoretical calculation is shown in Fig. 1. All the unbound levels above the α-decay threshold (dotted line) are identified by imposing the absorbing boundary condition (ABC), which is explained in a later section. Due to Pauli's exclusion principle between α and ${}^{16}\mathrm{O}$, the relative wave function of $\alpha - {}^{16}\mathrm{O}$ must have the total oscillator quanta of $N \geqslant 8$ when the nuclear potential is approximated to the harmonic oscillator potential [8]. Here the total oscillator quanta is given by the relation of $N = 2n + L$, in which n and L are the radial node number and the orbital spin in the $\alpha - {}^{16}\mathrm{O}$ relative wave function, respectively.

In Fig. 1, the bands of $N = 8$, 9, and 10 are shown. The $N = 8$ and 10 bands have the even orbital spin, while $N = 9$ has the odd orbital spin. The $N = 10$ band corresponds to the one higher nodal band of the ground $N = 8$ band. The present calculation using the potential model nicely reproduces the overall feature of the observed rotational bands. The moment of inertia is a little overestimated in the calculation of the $N = 8$ band ($L^{\pi} = 0^{+} \sim 6^{+}$), but the level spacing of the excited bands of $N = 9$ and $N = 10$ are nicely reproduced. The result of the present calculation is consistent with the result of the $\alpha + {}^{16}\mathrm{O}$ OCM calculation with the complex scaling method [21].

Second, the nuclear potential of $\alpha + {}^{15}\mathrm{O}$ is constructed by tuning the $\alpha + {}^{16}\mathrm{O}$ nuclear potential. The potential of $\alpha + {}^{16}\mathrm{O}$ is modified so as to reproduce the angular distribution of the $\alpha + {}^{15}\mathrm{N}$ elastic scattering. Comparison of the calculations with the experiments is shown in Fig. 2. The scattering calculation is done by the computational code of Automatic Local Potential Search (ALPS) [27]. We have calculated the differential cross section in the energy range from $E_{\alpha} = 6.85$ MeV to

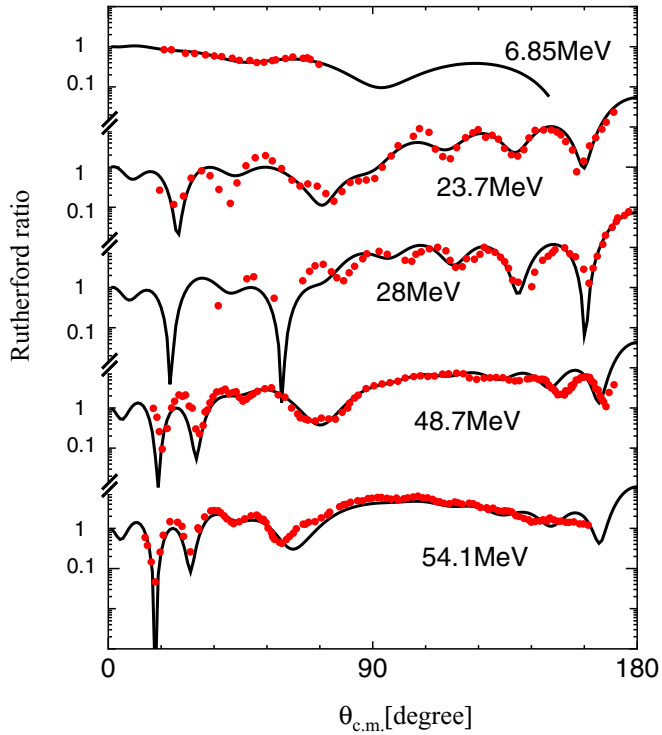

FIG. 2. (Color online) Differential cross sections of the $\alpha + {}^{15}$N elastic scattering. The dots show the experimental data, while the solid curves represent the theoretical calculation. The differential cross sections are plotted in the Rutherford ratio.

$E_\alpha = 54.1$ MeV. In this scattering calculation, only the depth of the WS potential is changed to $V = -166.31$ MeV, and the other parameters are unchanged. The real WS potential is energy independent, while the energy-dependent imaginary potentials, which combine the volume (V) and derivative (D) WS form factors, are introduced. The parameters of the imaginary potentials are listed in Table I. By introducing the energy-dependent imaginary potential, the theoretical calculation nicely reproduces the observed angular distribution over a whole range of the collision energy.

Third, the spectra of $^{19}\text{Ne} = \alpha + {}^{15}\text{O}$ is calculated from the nuclear potential of $\alpha + {}^{15}$N with an additional Coulomb force. Here we introduce the spin-orbit potential, which has the WS derivative form, $V_{LS}(r) = V_{LS} e^x (1 + e^x)^{-2}$ with $x = (r - R)/a$. In this calculation, R and a are fixed to the same values as those adopted to ^{20}Ne, and the strength parameter of V_{LS} is fixed to reproduce the binding energy of the lowest three negative parity states ($1/2^-_1$, $5/2^-_1$, and $3/2^-_1$) as much as possible. The resultant strength is $V_{LS} = -0.3$ MeV.

TABLE I. Parameters of the imaginary Woods-Saxon potential. W_I, R_I, and a_I represent the depth, radius, and diffuseness parameters, respectively, while the subscripts V and D denote the volume and derivative WS form factors, respectively. Ws and E_α (a_I and R_I) are in units of MeV (fm).

E_α	W_{IV}	R_{IV}	a_{IV}	W_{ID}	R_{ID}	a_{ID}
6.85	1.90	5.45	0.70	5.13	4.17	0.60
23.7	2.96	2.59	0.62	6.27	3.43	0.57
28.0	5.80	2.59	0.70	5.30	2.71	0.50
48.7	4.15	2.22	0.66	6.91	3.70	0.70
54.1	3.00	1.43	0.30	9.61	3.80	0.66

B. Absorbing and scattering boundary conditions

The energy spectra are calculated by the basis expansion method. The shifted Gaussian, having a form of $re^{-\nu(r-S)^2}$, is employed as the basis function in the calculation of the reduced radial wave function of $rR(r)$. In the basis function, the width parameter ν is 3.8 fm^{-2}, while the distance parameter S ranges from $S_{\min} = 0.1$ fm to $S_{\max} = 40.1$ fm with a constant mesh of $\Delta S = 0.5$ fm. Above the α-decay threshold, the absorbing boundary condition (ABC) [22–24] is applied to identify the resonance parameters, such as the resonance energy E_R and the decay width Γ_R. As for the absorbing potential, we employ the shifted polynomial function with a step function $\theta(x)$ like

$$W(r) = \theta(r - r_a)(r - r_a)^p. \quad (1)$$

Here r_a represents a starting point of the absorber, and $r_a = 12$ fm is used. The power of the polynomial is basically set to $p = 4$, while $p = 1$ and 2 are used to identify resonances appearing at the excitation energy close to the α threshold [23].

The excitation function of the $\alpha + {}^{15}$O elastic scattering is also calculated. In solving the scattering problem, we apply the Kohn-Hulthén-Kato (KHK) variational method [23,24,28,29]. In the present calculation, the computational procedure is the same as the method with the trial function (II) in Ref. [29]. The width parameter is $\nu = 4.0$ fm^{-2}, while the matching radius R_C is taken to be 12.0 fm. The distance parameters are $S_{\min} = 0.1$ fm, $S_{\max} = 14.1$ fm and $\Delta S = 0.35$ fm.

III. RESULTS

A. Negative-parity spectra

In the calculation of the negative-parity state of $\alpha + {}^{15}$O, an internal state of ^{15}O is frozen to be the $0p_{1/2}$ neutron hole configuration in ^{16}O, and we assume that the relative motion of $\alpha + {}^{15}$O has the $N = 8$ oscillator quanta, which is the same value as the ground rotational band in ^{20}Ne. We assign the $1/2^-_1$ state at -3.25 MeV to the ground state of $\alpha + {}^{15}$O with $L = 0$, while the $5/2^-_1$ at -2.02 MeV and $3/2^-_1$ at -1.91 MeV states are assumed to be the LS splitting states with $L = 2$, generated from the $N = 8$ state in ^{20}Ne. Here the binding energies are measured from the α threshold. The strength of the spin-orbit potential is fixed so as to reproduce the binding energies of these three levels.

The present identification of the calculated spectra is similar to the analysis of $^{19}\text{F} = \alpha + {}^{15}$N, which corresponds to the $1/2^-$ proton hole system of $\alpha + {}^{16}$O [8–10]. According to the coupled channel analysis of $(t + {}^{16}\text{O}) + [\alpha + {}^{15}\text{N}(1/2^-, 3/2^-)]$ in Ref. [10], these configurations are mixed with each other, but the $N = 8$ band of $\alpha + {}^{15}\text{N}(1/2^-)$ is clearly identified in the energy spectra of ^{19}F. In the low-lying states, for instance, $1/2^-_1$ (-3.90 MeV) is identified with $L = 0$, while the $5/2^-_1$ (-2.67 MeV) and $3/2^-_1$ (-2.56 MeV) states are assigned to the splitting state with $L = 2$. The energy

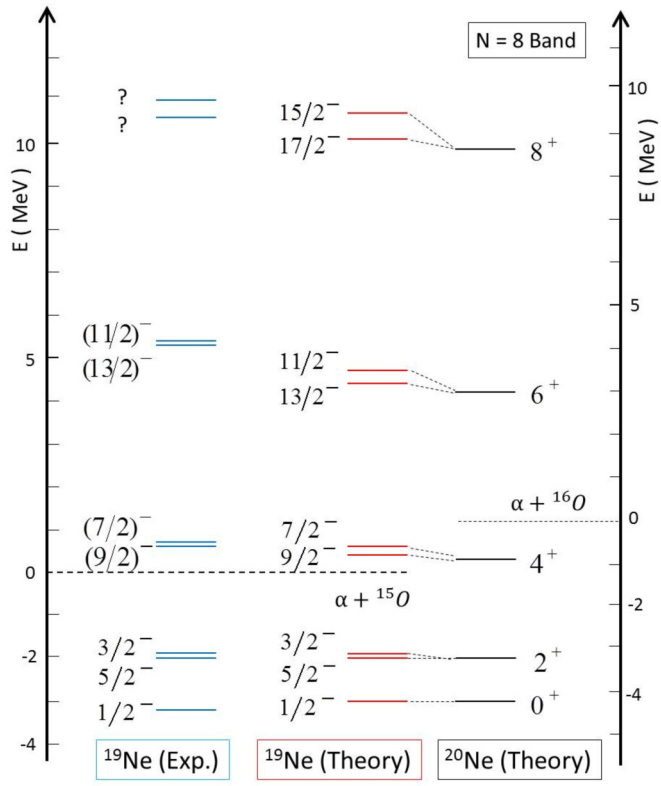

FIG. 3. (Color online) Energy spectra of ^{19}Ne with the negative parities ($N = 8$ and even L). The levels at the left side show the experimental spectra, while the middle and right levels show the theoretical calculations for ^{19}Ne($= \alpha + {}^{15}$O) and ^{20}Ne($= \alpha + {}^{16}$O), respectively. The LS splitting states of ^{19}Ne from ^{20}Ne are indicated by the dotted lines.

spacing of these three levels in ^{19}F is quite similar to those in ^{19}Ne. Thus, the identification of $\alpha + {}^{15}$O to the three bound levels, $1/2^-_1$, $5/2^-_1$ and $3/2^-_1$, is expected to be valid.

Comparison of the observation with the theory is shown in Fig. 3. The theoretical calculation (middle levels) nicely reproduce the observed bound levels (left levels), $1/2^-_1$, $5/2^-_1$, and $3/2^-_1$. In the unbound region, the spin-orbit splitting states in ^{19}Ne, building on the $N = 8$ rotational band of ^{20}Ne (right levels), are clearly predicted. The decay width of all the levels is quite small, and hence the levels are plotted by the single bars ($\Gamma_R < 10^{-3}$ MeV). Since the strength of the spin orbit interaction is very small ($V_{LS} = -0.3$ MeV), the energies of the LS splitting are also very small in the whole energy levels. At the left side in Fig. 3, some candidates of the observed levels, which seem to correspond to the theoretical calculation, are also plotted. Since the spin parities in the highly excited region have not been identified experimentally, the determination of the spin parity in experiments is very interesting.

We have also calculated the $N = 10$ band in ^{19}Ne, which corresponds to the one higher nodal band of $N = 8$. However, the width of the $N = 10$ resonances are very broad in comparison to that of the $N = 8$ band (typically, $\Gamma_R \sim$ a few MeV). Thus, the $N = 10$ resonances are embedded in the background continuum when we calculate the excitation function of the $\alpha + {}^{15}$O elastic scattering, which is discussed in a later section.

B. Positive parity spectra

The calculation for the $N = 9$ band in ^{19}Ne is shown in Fig. 4. In the $N = 9$ band, the resonant states have the visible width in contrast to the result of the $N = 8$ band. Thus, the resonant states are shown by the lines in the shaded area. The theoretical calculation of ^{19}Ne (middle levels) predicts the overlap of the LS-splitting states, generated from ^{20}Ne (right levels). However, the experimental information, especially in the higher energy region, is still insufficient, and future experiments are strongly desired.

The theoretical energy of $3/2^+$ is higher by about 2 MeV than the $3/2^+$ state observed at $E_x = 4.03$ MeV (the lowest level at $E = 0.5$ MeV in the left group), which is the most important in the astrophysical reaction of ^{15}O$(\alpha,\gamma)^{19}$Ne. This result is consistent with the result of the coupled-channel calculation of $(t + {}^{16}\text{O}) + (\alpha + {}^{15}\text{N})$ in ^{19}F [10]. In Ref. [10], the authors pointed out that the $3/2^+$ state just below the $\alpha + {}^{15}$N threshold in ^{19}F ($E_x = 3.91$ MeV), which is respective to the $3/2^+$ state at $E_x = 4.03$ MeV in ^{19}Ne, is out of the scope of the model that includes these two cluster configurations. As discussed in Refs. [15,16], the component of $\alpha + {}^{15}$N with the quanta of $N = 7$ or 9 is important in

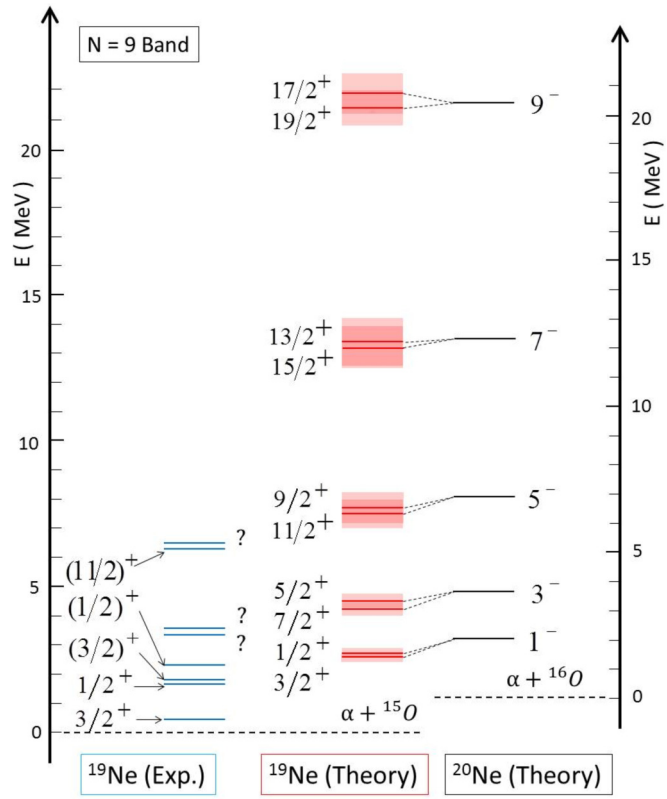

FIG. 4. (Color online) Same as Fig. 3, except for the $N = 9$ (odd L) band. The shade attached to the levels represents the decay width. See text for details.

the transfer reaction going to the $3/2^+$ state of ^{19}F. In ^{19}Ne, the corresponding $\alpha + {}^{15}$O cluster state is considered to be a minor mixture in the $5p$–$2h$ configuration with the hole state in $^{14}O_{g.s.}$ and the particle state in $^{21}Ne_{g.s.}$ [14]. Thus, the extended calculation, which takes into account the coupling of the $5p$–$2h$ and $\alpha + {}^{15}$O configurations explicitly, should be performed in a sophisticated analysis of the $3/2^+$ level at $E_x = 4.03$ MeV.

C. Excitation function of the $\alpha + {}^{15}$O resonant scattering

The excitation function of the $\alpha + {}^{15}$O elastic scattering is shown by the solid curve in Fig. 5. In this calculation, the scattering angle is fixed to $\theta_{c.m.} = 170^\circ$, which is almost the same condition as in the recent experimental setup [25]. The energy step is taken to be 0.01 MeV, which is much smaller than the experimental resolution (about 0.1 MeV) [25]. In this figure, the resonance energies are plotted by the solid circles, and the decay width of the individual resonances are shown by the error bars.

In the higher energy region of $E_{c.m.} \geqslant 2$ MeV, the three peaks of the positive parity resonances can be seen: $E_{c.m.} \sim 2.8$ MeV ($3/2^+$ and $1/2^+$), $E_{c.m.} \sim 4.0$ MeV ($7/2^+$ and $5/2^+$), and $E_{c.m.} \sim 8.0$ MeV ($11/2^+$ and $9/2^+$). The width of these resonances, identified by the ABC method, ranges from 0.2 to 1 MeV, and the resonance enhancements appear with the smooth energy variation. In contrast, the resonance width of the negative parity states, $13/2^-$ and $11/2^-$, are extremely sharp, and two sharp peaks are superposed on the broad bump appearing around $E_{c.m.} \sim 4$ MeV. There are two resonances of $9/2^-$ and $7/2^-$ in the lower energy region of $E_{c.m.} \leqslant 2$ MeV,

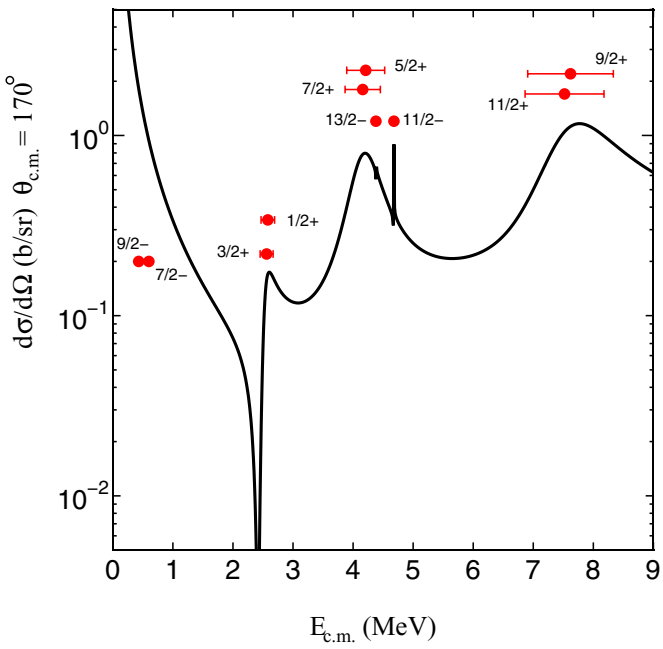

FIG. 5. (Color online) Excitation function of the $\alpha + {}^{15}$O elastic scattering at $\theta_{c.m.} = 170^\circ$. The solid curve shows the strength of the elastic scattering, while the solid circles show the energies of the resonant states identified by the ABC method. The error bars attached to the resonant levels represent the decay width.

but these resonances are completely masked by the enhanced background, arising from the kinematic factor of $E_{c.m.}^{-1}$ in the cross section. In the experiment of the $\alpha + {}^{15}$O elastic scattering, the resonance $1/2^+$ state is identified at $E_{c.m.} = 1.82$ MeV with $\Gamma_\alpha = 3.2 \pm 1.6$ keV [26]. The theoretical resonance of $1/2^+$ at $E_{c.m.} \sim 2.5$ MeV may correspond to the observed resonance although detailed analysis is needed in future studies.

Next, we investigate the validity of the experimental setup on the energy resolution and the detection angle [25]. If we smear the excitation function by the finite width of the experimental energy resolution, typically $\Delta E = 0.1$ MeV, the broad peaks for the positive-parity resonances are almost unchanged, but the sharp peak structures of the negative parities have completely disappeared. Thus, the negative-parity resonances will be difficult to observe in a realistic experiment. We also vary the detection angle in the range of $\theta_{c.m.} = 40^\circ$ to $\theta_{c.m.} = 180^\circ$. We have confirmed that the peak to valley structure becomes the most prominent in the angular region of $\theta_{c.m.} = 170^\circ \sim 180^\circ$. Therefore, the experimental setup for the energy resolution ($\Delta E = 0.1$ MeV) and the detection angle ($\theta_{c.m.} \sim 170^\circ$) are considered to be valid for the observations of the positive-parity resonances.

In the present calculation, we include only the cluster degrees of freedom and hence, other effects, which smear the resonant structures generated by the cluster configuration, should be considered. One of the smearing effects on the cluster resonances is originated from the coupling with a dozen of the low-J states (the levels of $J = 1/2$ or $3/2$), which are in the compound nuclear states. The theoretical estimation of the coupling effect is difficult, but a sharp resonance with $J^\pi = 1/2^+$ is identified in the experiment of the resonant scattering indeed [26]. Therefore, the smearing effect for the low-J state may be small in the excitation function shown in Fig. 5. To investigate the smearing effect more deeply, the coupling matrix elements between the cluster configurations and the compound states should be evaluated. The estimation of the coupling matrix is a subject for future study.

IV. SUMMARY AND DISCUSSION

In sum, we have calculated the rotational bands for ^{19}Ne and the excitation function of the $\alpha + {}^{15}$O elastic scattering based on the simple potential model of the $\alpha + {}^{15}$O system. The interaction potential of the $\alpha + {}^{15}$O system is constructed from the structural calculation of ^{20}Ne $= \alpha + {}^{16}$O and the $\alpha + {}^{15}$N elastic scattering. The calculation of ^{20}Ne nicely reproduces the observed spectra, and the $\alpha + {}^{16}$O potential is modified so as to reproduce the $\alpha + {}^{15}$N elastic scattering.

The present calculation predicts the rotational bands with the weak coupling scheme of a neutron hole in ^{16}O and the α particle. The qualitative feature of $\alpha + {}^{15}$O in ^{19}Ne is basically the same as that of $\alpha + {}^{15}$N in ^{19}F, which has already been justified by the coupled-channel study of $[\alpha + {}^{15}\mathrm{N}(1/2^-, 3/2^-)] + (t + {}^{16}\mathrm{O})$ [10] and the pioneering work in Ref. [8]. In the calculation of the $\alpha + {}^{15}$O elastic scattering, the scattering condition is set to the same condition as in the recent experiments [25]. Our calculation predicts the

appearance of the resonant structures in the excitation function. This result supports the experimental setup in Ref. [25].

In the present study, we have applied the simple potential model to the $\alpha + {}^{15}\mathrm{O}$ system. The potential model is useful for obtaining a schematic picture of the computational results, but, in future studies, we should perform the extended calculations, which include other cluster configurations. The ${}^{3}\mathrm{He} + {}^{16}\mathrm{O}$ cluster configuration is important because a considerable mixture of $t + {}^{16}\mathrm{O}$ and $\alpha + {}^{15}\mathrm{N}$ has already been pointed out in the mirror system, ${}^{19}\mathrm{F}$ [8,10]. Furthermore, the ${}^{5}\mathrm{He} + {}^{14}\mathrm{O}$ configuration, corresponding to the $5p$–$2h$ configuration in its shell-model limit, is essential in discussing the intrinsic structure of the $3/2^{+}$ resonance at $E_x = 4.03$ MeV [14,15]. Therefore, in a sophisticated calculation, we need to treat the sequential neutron transfers, such as ${}^{3}\mathrm{He} + {}^{16}\mathrm{O} \leftrightarrow \alpha + {}^{15}\mathrm{O} \leftrightarrow {}^{5}\mathrm{He} + {}^{15}\mathrm{O}$, and the treatment of the sequential transfers can be achieved on the basis of the ${}^{19}\mathrm{Ne} = {}^{3}\mathrm{He} + {}^{14}\mathrm{O} + 2N$ model. The generalized two-center cluster model (GTCM) is a powerful tool for handling such systems with two cores plus excess neutrons [4]. In fact, the GTCM has been successful in describing the structural problem [4] and the reaction problem [24,28] in Be isotopes with $\alpha + \alpha + XN$. Application of the GTCM to ${}^{19}\mathrm{Ne} = {}^{3}\mathrm{He} + {}^{14}\mathrm{O} + 2N$ is now in progress.

ACKNOWLEDGMENTS

We thank Y. Takenaka, K. Mimura, and all the members of the Theoretical Nuclear Physics Laboratory at Kansai University for their useful discussions and kind support. One of the authors (M.I.) thanks Prof. H. Yamaguchi at CNS for valuable discussions and useful comments.

[1] K. Ikeda *et al.*, Prog. Theor. Phys. Suppl. **68**, 1 (1980).
[2] H. Horiuchi *et al.*, Suppl. Prog. Theor. Phys. **192**, 1 (2012), and references therein.
[3] M. Freer, Rep. Prog. Phys. **70**, 2149 (2007).
[4] M. Ito, Phys. Rev. C **83**, 044319 (2011); M. Ito, N. Itagaki, and K. Ikeda, *ibid.* **85**, 014302 (2012); M. Ito, *ibid.* **85**, 044308 (2012).
[5] N. Itagaki, S. Okabe, K. Ikeda, and I. Tanihata, Phys. Rev. C **64**, 014301 (2001); N. Itagaki, T. Otsuka, K. Ikeda, and S. Okabe, Phys. Rev. Lett. **92**, 142501 (2004).
[6] M. Kimura, Phys. Rev. C **75**, 034312 (2007).
[7] T. Yamada and Y. Funaki, Phys. Rev. C **82**, 064315 (2010).
[8] B. Buck and A. A. Pilt, Nucl. Phys. A **280**, 133 (1977).
[9] F. Nemoto and H. Bando, Prog. Theor. Phys. **47**, 1210 (1972).
[10] T. Sakuda and F. Nemoto, Prog. Theor. Phys. **62**, 1274 (1979).
[11] K. Langanke *et al.*, Astrophys. J. **301**, 629 (1986).
[12] H. Scahtz *et al.*, Phys. Rep. **294**, 167 (1998).
[13] J. D. Garrett, R. Middleton, and H. T. Fortune, Phys. Rev. C **2**, 1243 (1970).
[14] H. T. Fortune, H. Nann, and B. H. Wildenthal, Phys. Rev. C **18**, 1563 (1978).
[15] Z. Q. Mao, H. T. Fortune, and A. G. Lacaze, Phys. Rev. Lett. **74**, 3760 (1995).
[16] Z. Q. Mao, H. T. Fortune, and A. G. Lacaze, Phys. Rev. C **53**, 1197 (1996).
[17] H. T. Fortune, Phys. Rev. C **68**, 034317 (2003).
[18] H. T. Fortune and R. Sherr, Phys. Rev. C **73**, 024302 (2006).
[19] H. T. Fortune, A. Lacaze, and R. Sherr, Phys. Rev. C **82**, 034312 (2010).
[20] K. Ikeda *et al.*, Prog. Theor. Phys. Suppl. Extra Number 464 (1968).
[21] A. T. Kruppa and K. Kato, Prog. Theor. Phys. **84**, 1145 (1990).
[22] H. Masui and Y. K. Ho, Phys. Rev. C **65**, 054305 (2002).
[23] M. Ito and K. Yabana, Prog. Theor. Phys. **113**, 1047 (2005).
[24] M. Ito, Phys. Lett. B **636**, 293 (2006); Mod. Phys. Lett. A **21**, 2429 (2006).
[25] H. Yamaguchi *et al.*, Phys. Rev. C **87**, 034303 (2013); **83**, 034306 (2011).
[26] F. Vanderbist *et al.*, Eur. Phys. J. A **27**, 183 (2006).
[27] Y. Iseri (private communication).
[28] M. Ito, N. Itagaki, H. Sakurai, and K. Ikeda, Phys. Rev. Lett. **100**, 182502 (2008); M. Ito and N. Itagaki, Phys. Rev. C **78**, 011602 (2008); M. Ito and K. Ikeda, Rep. Prog. Phys. **77**, 096301 (2014).
[29] M. Kamimura, Prog. Theor. Phys. Suppl. **62**, 236 (1977).